

Hydrothermal routes to various controllable morphologies of nanostructural lithium aluminate

Linfeng Hu^{*}, Bin Qiao, Zilong Tang, Zhongtai Zhang

*State Key Laboratory of New Ceramics and Fine Processing, Department of Materials Science and Engineering,
Tsinghua University, Beijing 100084, PR China*

Received 3 May 2006; received in revised form 5 November 2006; accepted 7 November 2006
Available online 18 December 2006

Abstract

The α -LiAlO₂ powders have been successfully prepared by a hydrothermal route based on using the surfactant of hexadecyltrimethyl ammonium bromide (CTAB) as the template. One-dimensional (1D) nanorods with higher and lower aspect ratio, 2D mesoporous microsheets were respectively observed with different concentration of the surfactants. A high specific surface area up to 151 m²/g was obtained by this method. The formation mechanism of the nanostructural lithium aluminate was proposed.
© 2006 Elsevier Ltd. All rights reserved.

Keywords: A. Nanostructures; B. Chemical synthesis; C. Electron microscopy; C. X-ray diffraction

1. Introduction

The development of nanoscience and nanotechnology requires precise control over the crystal structures, sizes and dimensionalities of materials in nanoscale. Up to now, many novel nanostructures have been successfully synthesized, such as nanotubes/nanowires/nanorods [1–3], and nanobelts [4]. Usually, a specific method might be applied to the synthesis of a certain class of materials that share similar crystal structures in nature; so it seems particularly important to study the formation mechanism of such materials under certain conditions.

Lithium aluminate (LiAlO₂) exhibits excellent thermo-chemical stability and favorable irradiation behavior. It is widely used as a matrix material in molten carbonate fuel cells (MCFC) and as a tritium-breeding material in nuclear fusion reactor [5,6]. Furthermore, the addition of 3 wt% 10 μ m LiAlO₂ particles into polymeric electrolyte of lithium secondary battery can enhance the ionic conductivity [7]. LiAlO₂ presents three different crystalline phases: α -, β - and γ -LiAlO₂, which are hexagonal, monoclinic and tetragonal, respectively. Wherein, γ -LiAlO₂ is the stable phase at high temperature, and α - or β -LiAlO₂ phases transform to γ -LiAlO₂ at an elevated temperature [8]. Previously, LiAlO₂ was prepared by conventional solid state methods, combustion synthesis or sol–gel methods [9–11]. High temperature and long time reaction were required in the solid state reactions, and the sol–gel method had a disadvantage in controlling the morphology of particles. Recently, LiAlO₂ particles with a high surface area of 45 m²/g, were prepared by a ultrasonic spray pyrolysis from an aqueous solution of aluminum nitrate and lithium salt [12]. Sokolov and Stein [13] synthesized LiAlO₂ with three dimensional periodic arrays of interconnected macropores by a colloidal crystal templating (PMMA)

^{*} Corresponding author. Tel.: +86 10 62772623; fax: +86 10 62772623.
E-mail address: hlf05@mails.tsinghua.edu.cn (L. Hu).

wet chemical process, of which the surface area was $56 \text{ m}^2/\text{g}$. However, these products contained some subsidiary substances and it was not easy to have high purity.

Presently, hydrothermal synthesis is normally applied for the preparation of different inorganic materials in a nanocrystalline state, such as mesoporous silicon [14], MgO nanorods [15], carbon nanotubes [16]. Here we reported a hydrothermal method for preparation a series of nanostructural $\alpha\text{-LiAlO}_2$ in controllable morphologies using a single-chain cationic surfactant (CTAB) as template. 1D nanorods with higher and lower aspect ratio, 2D mesoporous microsheets were respectively obtained by the method of changing the concentration of the surfactant. The specific surface area of the hydrothermal product was much higher than the reported results. The synthesis procedure provided a simple method to prepare nanostructure lithium aluminate.

2. Experiment

The starting materials selected were $\text{LiOH}\cdot\text{H}_2\text{O}$ (A.R.), aluminum *iso*-propoxide (AIP) (A.R.), CTAB (A.R.). The details of the preparation were indicated as follows: distilled water was added slowly to the mixture of $\text{LiOH}\cdot\text{H}_2\text{O}$, AIP and CTAB. The molar ratio of initial reagents for each sample was shown in Table 1. (The critical micelle concentration (CMC) value of CTAB at room temperature is $9.9 \times 10^{-4} \text{ M}$ [17].) The mixture was stirred 30 min with ultrasonic irradiation to obtain the homogeneous gel. Then the well-mixed gel was put into a Teflon autoclave vessel. The hydrothermal reaction was followed at 463 K under autogenous pressure for 10 h. The precursor was washed several times by absolute ethanol, dried at 353 K for 10 h, and then calcined at 773 K for 4 h in air.

A JEOL JEM-2011 transmission electron microscopy (TEM) with acceleration voltage of 200 kV and a JEOL JSM-6460LV scanning electron microscopy (SEM) were used to observe the morphology of the samples. The phase structure of the as-produced sample was characterized by a Bruker D8 advance X-ray diffractometer with monochromatized $\text{Cu K}\alpha$ radiation ($\lambda = 1.5418 \text{ \AA}$). The special-surface area was estimated by the Brunauer–Emmett–Teller (BET) four points method, on the basis of the nitrogen gas adsorption isotherm (77.4 K) with a NOVA4000 high gas sorption analyzer. The pore size distribution was also analyzed with the same apparatus.

3. Results and discussion

3.1. Phase structure

The LiAlO_2 phase was not found from the precursor that obtained after hydrothermal reaction in Fig. 1a. The precursor, composed of CTAB (JCPDS No. 48-2454), AIP (JCPDS No. 30-1508) and LiOH (JCPDS No. 01-1021), showed sharp and intense diffraction peaks, which indicated that precursor was well crystalline. The as-prepared samples after calcination at $500 \text{ }^\circ\text{C}$ can be characterized to be a hexagonal ($R\bar{3}m$) $\alpha\text{-LiAlO}_2$ phase (Fig. 1b), with lattice constants $a = 2.800 \text{ \AA}$ and $c = 14.18 \text{ \AA}$ (JCPDS No. 44-0024). This result demonstrated that starting materials did not change during the hydrothermal process and $\alpha\text{-LiAlO}_2$ phase was generated from the precursor during the heat-treatment stage. There were no significant differences in the wide-angle patterns between the samples of A–C. Compared with the precursor, the weak and broad diffraction peaks for the products suggested that the products might be composed of very small crystals with the size in nanoscale.

The insert of Fig. 1b was the small angle diffraction patterns for the precursor and the as-prepared sample C. The clear diffractions peaks at around 3.5° and 7° could be observed from the XRD patterns of the precursor, showing the uniform ordering of the pore structure. However, the XRD patterns of the sample C after calcination did not show any resolved diffraction peak, which implied absence of meso-structure order in the pore arrangement. This results showed that the uniformly meso-structured precursor has been obtained under the hydrothermal conditions because of the existence of the surfactant template. However, the ordering meso-structure was completely lost during the calcination process.

Table 1

The molar ratio of initial reagents for preparation of each sample

Sample	$\text{LiOH}\cdot\text{H}_2\text{O}$ (mmol)	AIP (mmol)	CTAB (mmol)	Distilled water (mmol)
A	600	600	0.050 (30 CMC)	100
B	600	600	0.860 (500 CMC)	100
C	600	600	5.180 (3000 CMC)	100

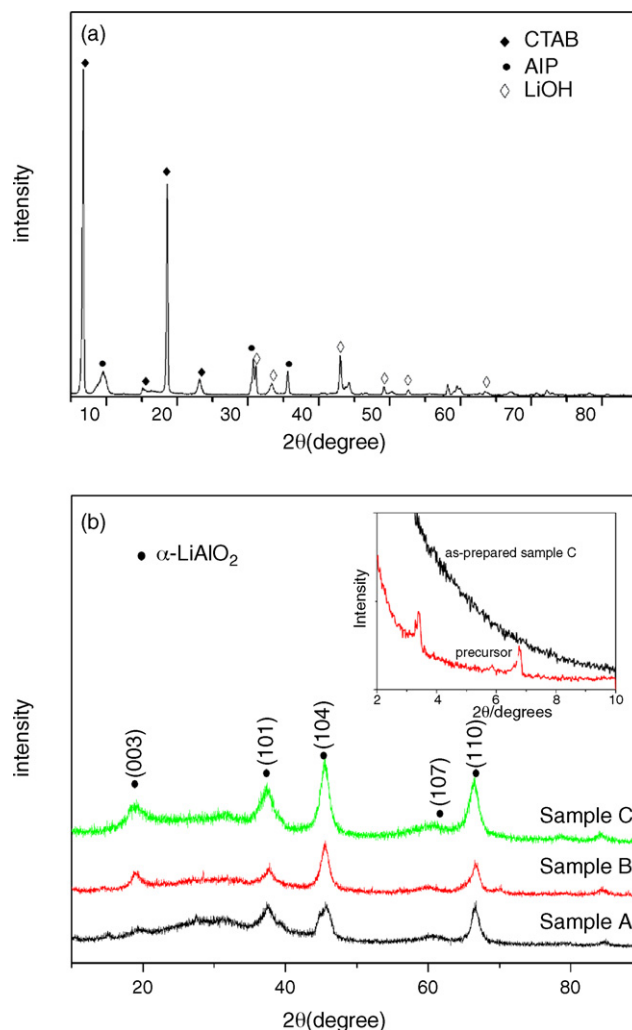


Fig. 1. XRD patterns for the precursor (a) and as-prepared samples (b). Insert is the small-angle diffraction pattern of sample C (precursor and as-prepared sample).

3.2. Morphologies

Representative TEM images for each sample were presented in Fig. 2. The morphologies of the products were different with the concentration of surfactants changed.

It was observed that the product powders of sample A exhibited a morphology of nanorods. The diameter of the nanorods was about 20–40 nm, with 150–300 nm in length, and aspect ratios (length/width) of about 4–7. The HRTEM micrograph of the sample showed the d_{112} interlayer spacing of nanorods was about 0.16 nm (see Fig. 2b), which was a little bigger than the literature values 0.14 nm (JCPDS No. 44-0024). The morphology of nanorods could also be found in the TEM images of sample B (Fig. 2c). However, these nanorods showed higher aspect ratio. The diameter of the nanorods for sample B was about 5–15 nm, and their lengths varied from 150 nm to 500 nm, with the length/width ratio about 30 (see in Fig. 2d). Moreover, among the nanorods of sample A and B, it seemed that some nanosheets could be found. Sample C displayed a micrograph of only thin rectangular microsheets, with 2.25 μm and 1.85 μm in width and length, respectively (Fig. 2e). From the HRTEM image for sample B, many disordered mesopores (pore size about 5–7 nm) were found on the microsheet (Fig. 2f). The selected-area electron diffraction (SAED) patterns of sample C showed the whole microsheet a single crystal structure. The SEM image for sample C was shown in Fig. 3, which indicated the thickness of the microsheet was 95 nm, approximately.

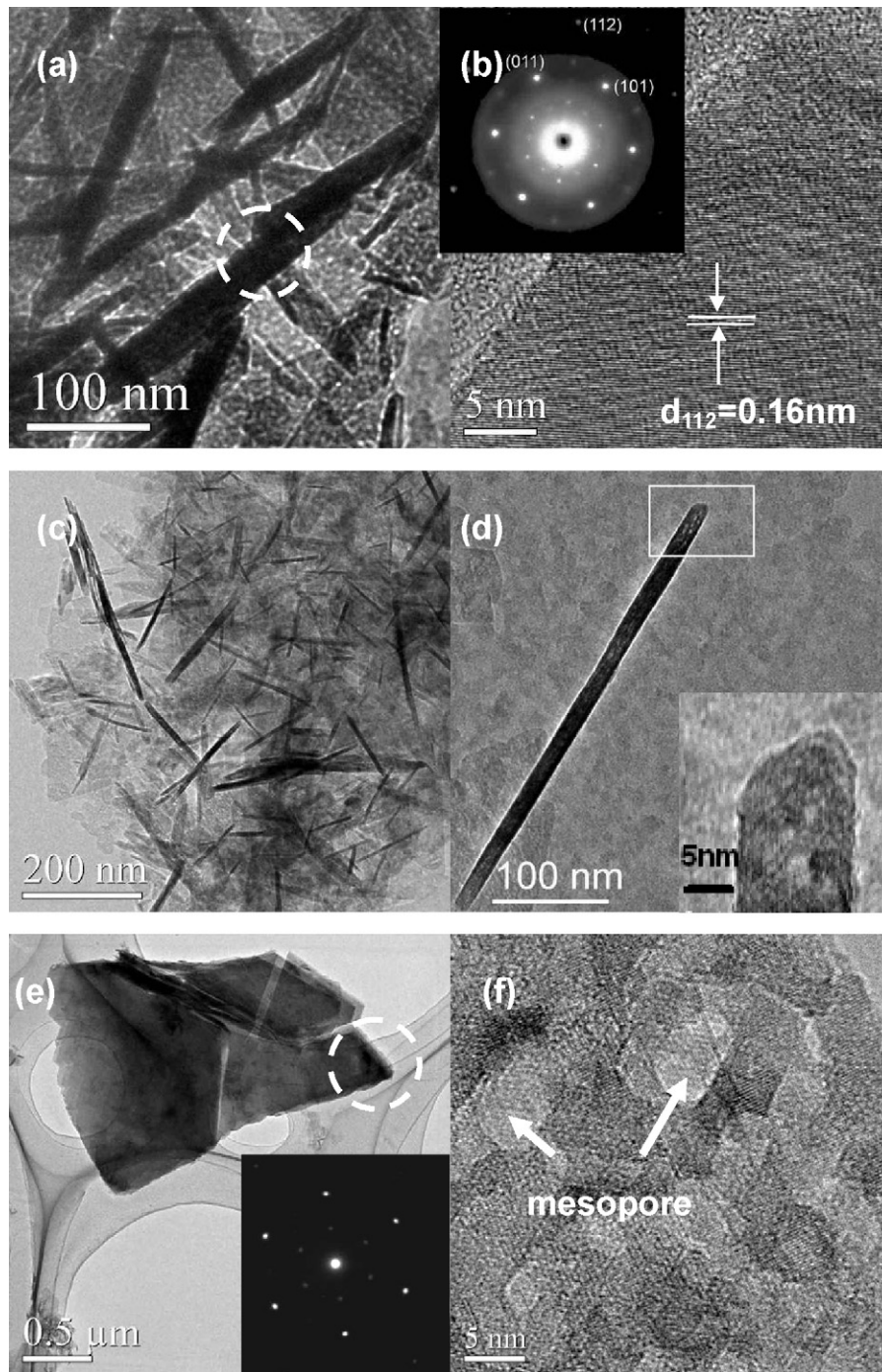


Fig. 2. Typical TEM micrographs of the samples with the selected area electron diffraction (SAED) pattern inserted.: (a) The nanorods image for sample A. (b) HRTEM image for sample A. (c) The nanorods with higher aspect ratio micrograph for sample B. (d) TEM image of an individual nanorod for sample B, with the HRTEM image inserted. (e) The microsHEET structure for sample C. (f) HRTEM image of sample C.

3.3. Specific surface area and pore distribution

Specific surface area of the samples was calculated according to nitrogen adsorption measurements. The specific surface area of samples A–C was $124 \text{ m}^2/\text{g}$, $143 \text{ m}^2/\text{g}$ and $151 \text{ m}^2/\text{g}$, respectively, all of which were much higher than

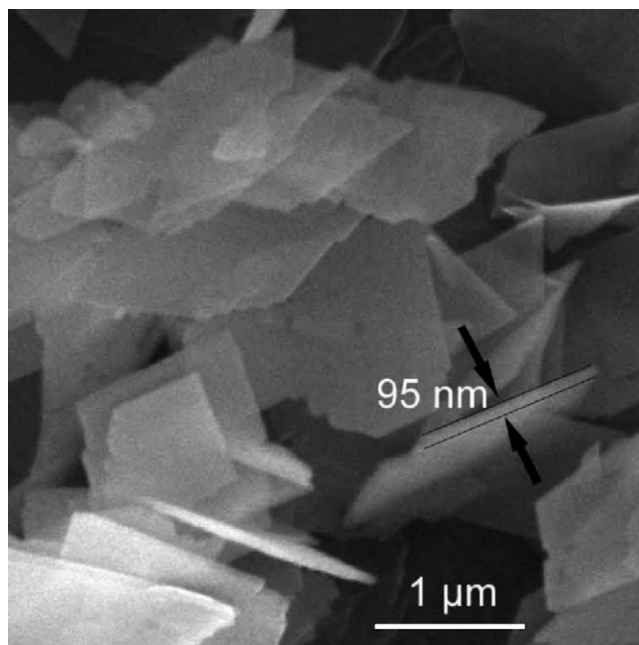


Fig. 3. SEM image for the sample C.

the reported results [12,13]. Sample C, as a typical example, its isotherm of nitrogen adsorption and desorption (Fig. 4) demonstrated the typical diffusion bottleneck structure, which exhibited large hysteresis loop of type E with sloping adsorption branch and steep desorption branch. The hysteresis type was due to the presence of different size of spheroidal cavities with the same entrance pore diameter, so the pore had a ink-bottle shape. The adsorption on isotherm at low pressure could be assigned to the monolayer coverage of particle surface, the adsorption at the medium pressure ($p/p_0 = 0.4$ – 0.85) mainly due to capillary condensation of N_2 in mesopores, while at the high pressure ($p/p_0 = 0.85$ – 0.99) it was likely contributed by aggregated pores. Pore size distribution was then determined by the Brunauer–Joyner–Halenda (BJH) method. A narrow mesopore size distribution, 4–7 nm was achieved, which was

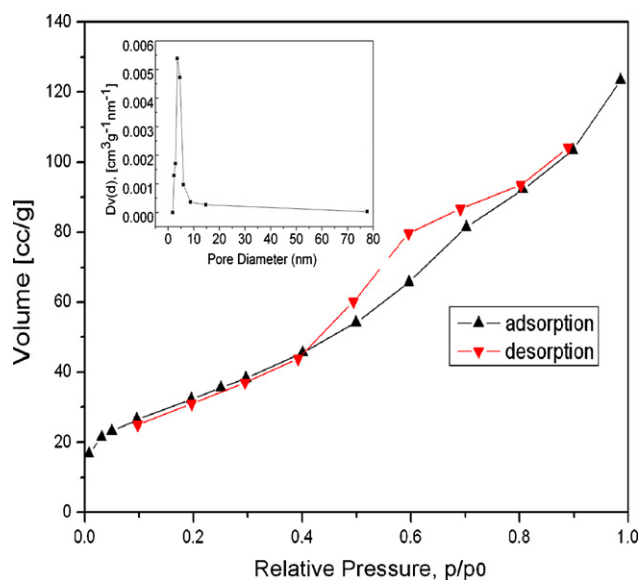


Fig. 4. Nitrogen adsorption–desorption isotherms and pore size distribution of sample C.

quite consistent with the result estimated from the TEM micrograph in Fig. 2. The whole pore volume of sample C was $0.1769 \text{ cm}^3/\text{g}$.

3.4. The formation mechanism analysis

It was clear that the starting materials were not changed during the hydrothermal reaction process, so lithium aluminate phase was produced at the calcination stage. Since the formation mechanism of lithium aluminate nanostructures is not completely clear, an assumed interpretation for the observed nanostructures can be stated as follows:

It was known that molecules of CTAB aggregated as templates when the concentration was beyond CMC. For samples A and B, surfactants formed nanocapsules micelle templates and LiOH and AIP were packaged in the capsules. During the heat treatment process, the surfactants were decomposed so the nanorods were formed. Meanwhile, the precursor converted to $\alpha\text{-LiAlO}_2$. The length of nanocapsule depended on the surfactant concentration, that is, low surfactant concentration favored shorter and thicker micelles and high surfactant concentration favored longer and thinner micelles. In the starting materials, the surfactant concentration for sample B ($n_{\text{CTAB}} = 500 \text{ CMC}$) was higher than sample A ($n_{\text{CTAB}} = 30 \text{ CMC}$). For this reason, sample A showed nanorods micrograph with lower aspect ratio, and sample B presented nanorods micrograph with higher aspect ratio. This proposed model was supported by the other observations from the synthesis of MCM-41 silica [18]. The proposed formation mechanism of the nanorods of lithium aluminate was illustrated schematically in Fig. 5a.

When the surfactant concentration was up to much higher, such as 3000 CMC for sample C, the formation of the mesoporous microsheets may be suggested in a different way. According to the theory of Jeffrey SB [19], molecules of CTAB aggregated as lamellar liquid crystal template. The molecule of CTAB was consisted of two tails: one was the worm-like hydrophobic headgroup, and the other was the ball-like hydrophilic headgroup. All the hydrophilic headgroups aggregated together at one side of the layer, and all the hydrophobic aggregated at another side, so the layer had a ball-like side and a worm-like side. Then LiOH and AIP accumulated at the ball-like side of the lamellar liquid crystal template and also formed a layer shape (called LiOH-AIP layer). Enlargement of one single crystal of

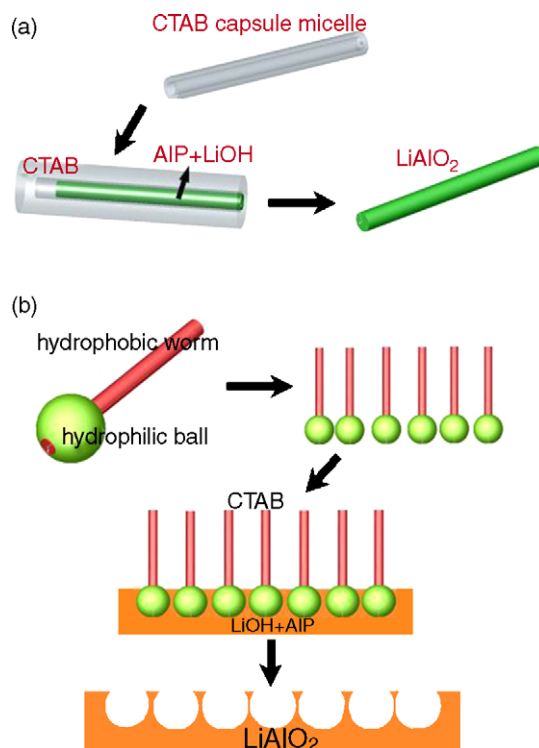


Fig. 5. Proposed formation mechanism of the nanorods (a) and mesoporous microsheets (b) of lithium aluminate.

LiOH-AIP layer resulted in the products with highly regular shape (rectangular shape). Under the autogenous pressure of hydrothermal process, the molecules of CTAB could be removed more easily, which led to the LiOH-AIP layer with long-range ordered porosity. Finally, surfactants were eliminated and the long-range ordering was destroyed by calcination, many ink-bottle cylindrical pores were formed, which was in great agreement with the result of N₂ adsorption analysis. Fig. 5b illustrated schematically the proposed formation mechanism of the mesoporous microsheets.

4. Conclusions

In summary, we have succeeded in controllable synthesizing of 1D nanorods/2D mesoporous microsheets α -LiAlO₂ by controlling the concentrations of the surfactant CTAB. LiAlO₂ nanorods with low and high aspect ratio were respectively prepared when the surfactant concentration is 30 CMC, 500 CMC. When the surfactant concentration was up to much higher such as 3000 CMC, mesoporous microsheets were obtained, which show a high specific surface area of 151 m²/g. The value of surface area was much higher than the reported results.

Acknowledgements

Authors gratefully acknowledge the support of National Natural Science Funds of China (Grant Nos. 50472005 and 50372033), as well as the Basic Research Funds of Tsinghua University (Grant No. JC 2003040).

References

- [1] L.H. Qu, C.Q. He, Y. Yang, *Mater. Lett.* 59 (2005) 4034.
- [2] J.R. Li, Z.L. Tang, Z.T. Zhang, *Electrochem. Commun.* 7 (2005) 62.
- [3] T.Z. Ren, Z.Y. Yuan, B.L. Su, *Chem. Phys. Lett.* 374 (2003) 170.
- [4] Y.J. Li, L.P. You, R. Duan, *Solid State Commun.* 129 (2004) 233.
- [5] S. Terada, I. Nagashima, K. Higaki, *J. Power Sources* 75 (1998) 223.
- [6] M. Nishikawa, T. Kinjyo, S. Beloglazov, *J. Nucl. Mater.* 335 (2004) 70.
- [7] M. Morita, T. Fujisaki, M. Yoshimoto, *Electrochim. Acta* 46 (2001) 1565.
- [8] R.A. Ribeiro, G.G. Silva, N.D.S. Mohallem, *J. Phys. Chem. Solids* 62 (2001) 857.
- [9] G.Y. Hou, J. Zang, Y.L. Wang, *Rare Met. Mater. Eng.* 33 (2004) 1351.
- [10] F. Li, K. Hu, J.L. Li, *J. Nucl. Mater.* 300 (2002) 82.
- [11] F. Oksuzomer, S.N. Koc, I. Boz, *Mater. Res. Bull.* 39 (2004) 715.
- [12] Y.C. Kang, S.B. Park, *J. Colloid Interface Sci.* 182 (1996) 59.
- [13] S. Sokolov, A. Stein, *Mater. Lett.* 57 (2003) 3593.
- [14] W.Z. Zhou, J. Klinowski, *Chem. Phys. Lett.* 292 (1998) 207.
- [15] Y. Li, Z. Jing, Y.D. Li, *Mater. Chem. Phys.* 76 (2002) 119.
- [16] W.Z. Wang, J.Y. Huang, D.Z. Wang, *Carbon* 43 (2005) 1317.
- [17] K. Cui, Q. Cai, X.H. Chen, *Micropor. Mesopor. Mater.* 68 (2004) 63.
- [18] Q. Cai, Z.S. Luo, F.Z. Cui, *Chem. Mater.* 13 (2001) 262.
- [19] S.V. Jeffrey, C.V. James, *J. Colloid Interface Sci.* 269 (2004) 394.